Earth and Planetary Science Letters 427 (2015) 1–10

Contents lists available at ScienceDirect

Earth and Planetary Science Letters

www.elsevier.com/locate/epsl

Dynamic triggering of creep events in the Salton Trough, Southern California by regional M ≥ 5.4 earthquakes constrained by geodetic observations and numerical simulations

Meng Wei [a,*], Yajing Liu [b], Yoshihiro Kaneko [c], Jeffrey J. McGuire [d], Roger Bilham [e]

[a] University of Rhode Island, Narragansett, RI, USA
[b] McGill University, Montréal, Québec, Canada
[c] GNS Science, Lower Hutt, New Zealand
[d] Woods Hole Oceanographic Institution, Woods Hole, MA, USA
[e] University of Colorado Boulder, Boulder, CO, USA

ARTICLE INFO

Article history:
Received 20 February 2015
Received in revised form 22 June 2015
Accepted 25 June 2015
Available online 10 July 2015
Editor: P. Shearer

Keywords:
dynamic triggering
creep events
shallow frictional heterogeneity
amplitude threshold
Superstition Hills Fault

ABSTRACT

Since a regional earthquake in 1951, shallow creep events on strike-slip faults within the Salton Trough, Southern California have been triggered at least 10 times by M ≥ 5.4 earthquakes within 200 km. The high earthquake and creep activity and the long history of digital recording within the Salton Trough region provide a unique opportunity to study the mechanism of creep event triggering by nearby earthquakes. Here, we document the history of fault creep events on the Superstition Hills Fault based on data from creepmeters, InSAR, and field surveys since 1988. We focus on a subset of these creep events that were triggered by significant nearby earthquakes. We model these events by adding realistic static and dynamic perturbations to a theoretical fault model based on rate- and state-dependent friction. We find that the static stress changes from the causal earthquakes are less than 0.1 MPa and too small to instantaneously trigger creep events. In contrast, we can reproduce the characteristics of triggered slip with dynamic perturbations alone. The instantaneous triggering of creep events depends on the peak and the time-integrated amplitudes of the dynamic Coulomb stress change. Based on observations and simulations, the stress change amplitude required to trigger a creep event of a 0.01-mm surface slip is about 0.6 MPa. This threshold is at least an order of magnitude larger than the reported triggering threshold of non-volcanic tremors (2–60 kPa) and earthquakes in geothermal fields (5 kPa) and near shale gas production sites (0.2–0.4 kPa), which may result from differences in effective normal stress, fault friction, the density of nucleation sites in these systems, or triggering mechanisms. We conclude that shallow frictional heterogeneity can explain both the spontaneous and dynamically triggered creep events on the Superstition Hills Fault.

1. Introduction

Static stress changes associated with a large earthquake decrease with the distance from the hypocenter much faster than do peak dynamic stress changes (Cotton and Coutant, 1997). Therefore it is usually assumed that dynamic perturbations are the main cause for triggering earthquakes outside the aftershock zone (<~2 fault lengths of the epicenter). Within the aftershock zone, it is believed that both static and dynamic stresses can trigger aftershocks, even though it is still debated which mechanism is more important and likely to explain both instantaneous triggering and delayed triggering (Kilb et al., 2000; Freed, 2005; Richards-Dinger et al., 2010). The static stress changes associated with Coulomb stress change $\Delta\sigma_f$ accompanying fault slip ($\Delta\sigma_f = \Delta\tau + f\Delta\sigma$, where $\Delta\tau$ is the shear stress change, f is the coefficient of friction, and $\Delta\sigma$ is the normal stress change) can account for some aftershock activity (Stein, 1999). However, a large volume of literature based on observations, numerical modeling, and lab experiments reveals that dynamic triggering involves numerous contributory phenomena, such as mainshock magnitude, proximity, amplitude spectra, peak ground motion, and mainshock focal mechanisms (Gomberg et al., 1998; Perfettini et al. 2003a, 2003b; Brodsky and Prejean, 2005; Johnson et al., 2008). Moreover, in a recent review of the response to 260 M ≥ 7.0 shallow (depth <50 km) mainshocks in 21 global regions with local seismograph

* Corresponding author at: Graduate School of Oceanography, University of Rhode Island, Narragansett, RI 02882, USA.
E-mail address: matt-wei@uri.edu (M. Wei).

http://dx.doi.org/10.1016/j.epsl.2015.06.044
0012-821X/

networks, Parsons et al. (2014) concluded that the aforementioned factors may not be the dominant ones for dynamic triggering of earthquakes and rather, azimuth and polarization of surface waves with respect to receiver faults may play more important roles.

Stress changes accompanying a large earthquake not only trigger other earthquakes but also induce aseismic slip on strike-slip faults. A creep rate reduction on the southern Hayward fault after the 1989 Loma Prieta earthquake is consistent with the reduction of shear stress induced by the earthquake (Lienkaemper et al., 2001). The 1983 Coalinga earthquake appeared to have affected the creep rate on the creeping section of the San Andreas Fault near Parkfield in a similar manner (Simpson et al., 1988). Du et al. (2003) calculated the static stress change due to nearby earthquakes in the Salton Trough, Southern California. They found in 7 out of 10 cases static stress changes promoted triggered slip. In a numerical simulation they applied sinusoidal waves to a single-degree-of-freedom spring-slider system to study the effect of dynamic triggering on fault creep. They showed that certain types of transient loads can trigger a creep event. However, the dynamic stress perturbations introduced in their simulation are hypothetical sinusoidal waves and their model does not have depth-dependent fault properties, and hence the model results cannot be directly compared to natural fault slip observations.

Recent advances in observations and numerical simulations encourage us to revisit the topic to improve our understanding of creep events triggering by nearby large earthquakes. Wei et al. (2013) developed a numerical fault model that can explain geodetic and geological observations of spontaneous creep events on strike-slip faults. This model can be modified to simulate triggered creep events and compare them with observations. In addition, large amounts of seismic, strain and fault creep data are now available in the Salton Trough. We have a very good record of both the forcing function (strain changes from which we may infer stress changes) and the response of the fault, i.e. surface creep events with known amplitudes. The study of near surface triggering of fault slip is thus more precisely constrained than the study of triggered subsurface earthquakes or non-volcanic tremors, where the fault response occurs deep within the earth and where the location and time history of slip is rarely well constrained by geodetic data. In the absence of the time history of triggered slip the measured response is usually a rate change that poorly constrains mechanical models.

In this paper, we focus on the causal mechanism of episodic creep events on the Superstition Hills Fault (SHF) triggered by moderate earthquakes in and near the Salton Trough. Prior to the 24th November 1987, Mw 6.7 earthquake on the SHF, slip rates on the fault were less than 0.5 mm/yr (Louie et al., 1985). After 1987, more than 25 yr of surface afterslip has been recorded (Bilham, 1989; Rymer et al., 2002; Wei et al., 2011, 2013). To begin, we construct a comprehensive catalog of creep events on the SHF based on data from geological surveys, creepmeter and Interferometric Synthetic Aperture Radar (InSAR) measurements. Next, we constrain the static and dynamic perturbations on SHF from six $M \geq 5.4$ earthquakes based on published papers and strong motion data, respectively. Finally, realistic static and dynamic perturbations for the 1992 Mw 7.3 Landers, 1999 Mw 7.1 Hector Mine, and 2010 Mw 7.2 El Mayor were analyzed using the numerical fault model proposed by Wei et al. (2013).

2. Observations of creep events at Salton Trough, Southern California

On many creeping faults, surface creep consists of continuous creep and episodic creep events (Bilham, 1989; Wei et al., 2013). Creep events occur spontaneously, or during the passage of surface waves from nearby earthquakes (Rymer et al., 2002), or in response to soil moisture changes (Schulz et al., 1983). The Salton Trough is a sedimentary basin at the southern end of the San Andreas Fault system near the US and Mexico border. Records of triggered slip are available for more than ten occasions from the Superstition Hills Fault (SHF), the San Andreas Fault, and the Imperial Fault as well as from numerous minor faults in the Coachella and Imperial Valleys (Rymer et al., 2002; Wei et al., 2011, 2013). Since 1950, more than 10 earthquakes with $M \geq 5.4$ have occurred within 200 km from this region (Fig. 1), many of which triggered creep events on multiple faults (Table S1 in the supplementary material). From Table S1 it is evident that triggered surface slip can occur when the host fault lies within 150 km of a $Mw > 7$ earthquake, within 80 km of a $Mw > 6$ earthquake, or within 20 km of a $Mw > 5$ earthquake. Not all triggered slip occurs on faults recognized to be actively creeping, but in general those that exhibit steady slow surface creep or episodic creep events are regularly triggered by nearby earthquakes.

The SHF has over 60 yr of record of triggered creep as early as 1951 (Allen et al., 1972) and over 25 yr of digital data. Since 1951, creep events on the SHF were triggered by the 1968 Mw 6.5 Borrego Mountain, 1979 Mw 6.4 Imperial, 1981 Mw 5.8 Westmorland, 1992 Mw 7.3 Landers, 1999 Mw 7.1 Hector Mine, 2010 Mw 7.2 El Mayor (Rymer et al., 2002; Wei et al., 2011 and references therein), and the 2012 Mw 5.4 Brawley (Hauksson et al., 2013) earthquakes. The largest observed triggered creep event has a surface slip of 22 mm and the smallest of 0.17 mm (Table 1). Determining the exact timing and associated uncertainties of triggered creep depends on available measurements. For the seven earthquakes mentioned above, creepmeter measurements are available only for creep events triggered by the 1992 Landers and Big Bear earthquakes, the 2010 El Mayor and the 2012 Brawley earthquakes. Where data with a sample rate of 1 min were available in 1992 it appears that triggered slip accompanies the passage of surface waves (Bodin et al., 1994). The timing of creep associated with other earthquakes relies on field survey and InSAR, and therefore we can only confirm that creep occurred within 24 h after the mainshock.

The history of SHF creep events is complementarily constrained by geological surveys, creepmeter and InSAR measurements. Field survey on the SHF has been conducted since 1950s after each regional large earthquake (Rymer et al., 2002). An analogue creepmeter was installed on the SHF in 1967 by Caltech but it recorded negligible creep (Louie et al., 1985). Three digital creepmeters operated on the SHF for five years following the 1987 Mw 6.6 SHF earthquake (Bilham et al., 2004). Recording was resumed with a single creepmeter in March 2004. The sampling rate of a creepmeter is typically 1–5 min (Bilham et al., 2004). InSAR data became available following the launch of the ERS satellite in 1992, and the interval between ERS/Envisat InSAR observations is 35 days. Field surveys usually occur within 24 h of the mainshock (Rymer et al., 2002).

Aiming to find possible creep events during the 1992–2004 time period when the creepmeter was off-line, we analyzed ERS InSAR images (Track 356 Frame 2943, Fig. 2). The data were downloaded from the UNAVCO SAR archive and processed with GMTSAR (http://topex.ucsd.edu/gmtsar/). Based on the InSAR data, we infer that at least two previously unknown large events occurred between 1993 and 1996. Assuming most of the deformation is horizontal (there is no topographic step across the fault) we estimated a displacement of 1–2 cm for both events (Fig. 2). Robert Sharp (personal communication, 1999) observed one of these 2 cm events in the field but its time is not well resolved. The first event occurred between 11/03/1993 and 07/13/1995, and the second one occurred between 10/11/1996 and 12/20/1996. The timing of the second event is better constrained than the first event because more SAR images became available after the launch of ERS2

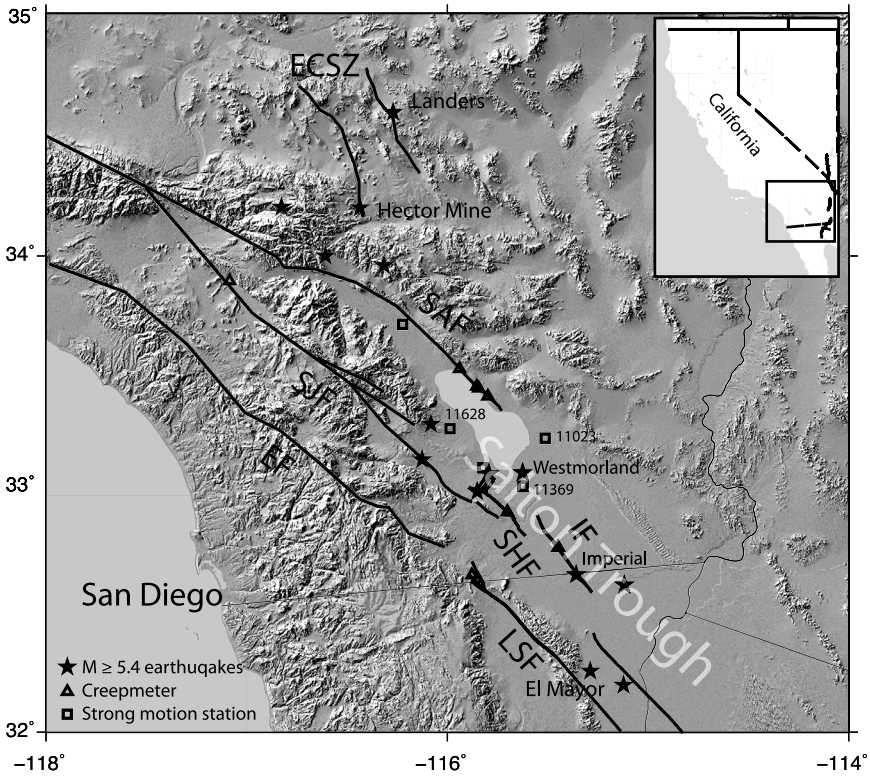

Fig. 1. Study area in Southern California. The Salton Trough is the region of low relief in the SE corner of the map. Stars show moderate ($M \geq 5.4$) earthquake epicenters with significant events labeled. Triangles are locations of creepmeters. Open squares show nearby strong motion stations (station number indicated). Fault names are abbreviated as following: Eastern California Shear Zone (ECSZ), San Andreas Fault (SAF), San Jacinto fault (SJF), Elsinore fault (EF), Superstition Hills fault (SHF), Imperial fault (IF), and Laguna Salada fault (LSF).

in 1995. Considering the magnitude and time range of these two creep events, it is likely that each episode was a single event, although, due to the InSAR time resolution, we cannot rule out the possibility that each consisted of multiple smaller events. Fig. 3 thus presents the most complete slip history of creep events on a strike-slip fault up to date. We also found two creep events that only slipped at the northern segment of SHF. We do not include them in the creep time series in Fig. 3 because the creepmeter is located in the southern segment of SHF. Many creep events occurred during 1988–1991 but there was only one case in that time period where a M4.7 likely triggered slip on SHF (Williams and Magistrale, 1989). Part of this is due to the paucity of $M > 4$ aftershocks (Bilham, 1989). There were only three $M > 4$ aftershocks since the installation of the creepmeters in December 1987, and the last one occurred in March 1988. Since then, there was no $M > 4$ earthquake on the SHF.

3. Observations and modeling of stress perturbations on the SHF

The static Coulomb stress changes on the SHF produced by nearby large earthquakes (Table 1 and references in the caption) are usually quite small (<0.1 MPa). Du et al. (2003) calculated the static Coulomb stress perturbations on the SHF to be less than 0.1 MPa for all major earthquakes before 1993. The static Coulomb stress change on the SHF generated by the 1992 Landers and 1999 Hector Mine earthquakes were less than 1 kPa (Fialko et al., 2002). For the 2010 Mw 7.2 El Mayor earthquake, the Coulomb stress change on the SHF is negative (−0.02 MPa) and therefore acts to inhibit creep events rather than triggering them (Toda and Stein, http://supersites.earthobservations.org/Baja_stress.png). For the 1968 Mw 6.5 Borrego Mountain, 1979 Mw 6.4 Imperial, 1981 Mw 5.8 Westmorland, the 2012 Mw 5.4 Brawley earthquakes, both static and dynamic stress perturbations seemed to have promoted creep events. The static Coulomb stress change at the southern segment of SHF is about 0.03, 0.03, 0.05 and 0.07 MPa, respectively (see references in Table 1). However, these numbers are 1–2 orders of magnitude smaller than the dynamic stress perturbations with the exception of the 2012 Mw 5.4 Brawley earthquake, which is very close to SHF. We will later show that these static stress changes are too small to trigger creep events. Instead, dynamic perturbations are the main mechanism of triggering creep events at SHF.

The dynamic stress changes were constrained mainly by strong motion data, which are available for many of the relevant events over the last 40 yr. A potential instrumental problem with strong motion sensors is that they are not designed to accurately record long period (>10 s) seismic waves (Boore and Bommer, 2005). With the notion that longer period perturbations might be the most important in triggering (Brodsky and Prejean, 2005), we used high-rate GPS data (Bock et al., 2011) to validate the use of strong motion data alone for computing dynamic stress perturbations in this region. The comparison between high-rate GPS (1 Hz) and strong motion and combined GPS-strong-motion shows that the strong motion sensor records very likely reflect the true ground motion for nearby large earthquakes in this region (Fig. S1 in the supplementary material). For consistency, we use strong motion data to constrain the dynamic perturbations even when high-rate GPS data are available for recent events. We primarily rely on the strong motion station 11 628 (30 km north of the northern end of SHF) because it is the longest running (since at least 1992) and the closest station to SHF (Fig. 1). The strong motion displacement time series are rotated to the normal and shear directions relative to the SHF fault plane, and translated respectively to normal and shear stress changes using the equation: $stress = \frac{dD}{dt} * \mu / V_g$, where D is the strong motion data in displacement, V_g is the group wave velocity (3.5 km/s), and μ is the shear modulus (30 GPa).

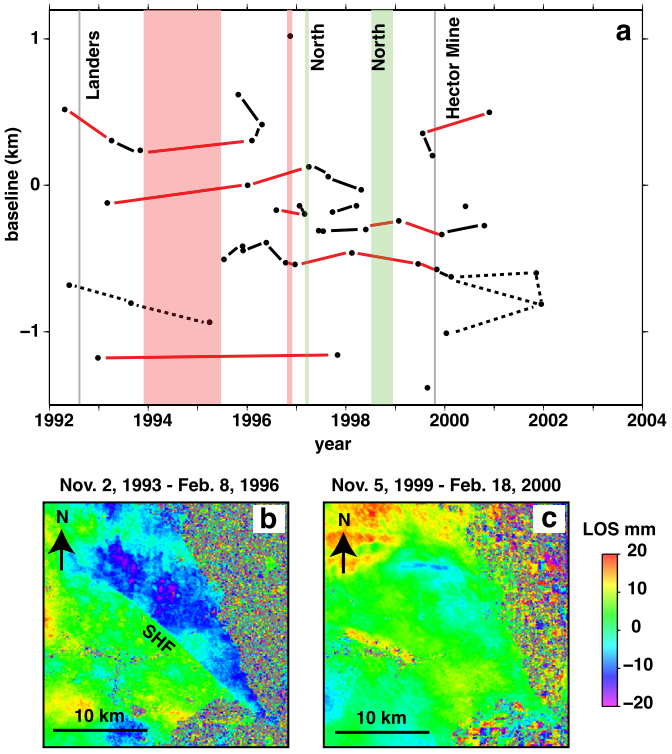

Fig. 2. InSAR data used to identify creep events on the SHF. (a) Time-baseline map of InSAR data used in this study. A baseline is the distance between the satellite positions when the SAR images were acquired. A short baseline ($< \sim 250$ m) is required to make interferograms. Red and black solid lines link the pairs that show or lack displacement on the SHF (phase change across the fault trace) respectively. Dashed black lines denote pairs with interferograms that were too noisy to determine fault motion. Pink rectangles highlight the possible time periods for the two newly identified creep events. Green rectangles highlight two events that slipped only at the northern segment of the SHF. (b) Example InSAR image showing slip on the SHF as indicated by the sharp boundary between the green region in the southwest and blue region in the northeast. The phase change across the SHF is caused by displacement on the fault. The cloudy blue area is likely water vapor noise. (c) Example InSAR image showing no slip on the SHF. The cloudy red area in the top-left corner is also water vapor noise. (For interpretation of the references to color in this figure legend, the reader is referred to the web version of this article.)

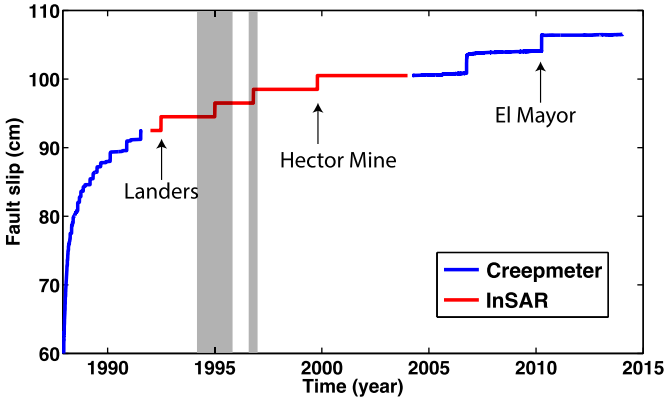

Fig. 3. Composite afterslip history on the Superstition Hills Fault at the location of the Imler Road creepmeter since 6 days after the 1987 Mw 6.7 SHF mainshock, based on creepmeter and InSAR data as well as field surveys. Field surveys provided ground-truth data for many creep events. The absolute amplitude of fault slip at the starting point of each time series is unknown. We aligned the three time series to form a continuous history. Gray bars show the range of possible occurrence times of the two newly identified creep events as constrained by InSAR data. Arrows point to creep events triggered by nearby large earthquakes.

This assumes that large amplitude surface waves are more important in triggering than body waves and that the surface waves can be treated as a plane wave with a constant velocity. All the earthquakes listed in Table 1 show a peak-to-trough amplitude of 0.5–1 MPa in dynamic perturbations at the Imler road site on the SHF and are at least an order of magnitude larger than static stress changes, with the exception of the 2012 Mw 5.4 Brawley earthquake, for which the static stress is as large as the dynamic stress perturbation.

4. Fault slip modeling in the framework of rate-and-state friction

We next model the SHF as a 1D strike-slip fault with depth-variable frictional properties in a 2D medium in the framework of laboratory-derived rate-and-state friction laws (Dieterich, 1979; Ruina, 1983). Wei et al. (2013) proposed a model that includes three layers of alternating frictional stability above the seismogenic zone (Fig. 4) because the traditional 3-layer model (Scholz, 1998) cannot simultaneously reproduce the continuous afterslip and the episodic creep events observed following the 1987 Mw 6.7 SHF earthquake. Specifically, a thin velocity-weakening (VW) layer is embedded within the top stable zone. As a result, creep events nucleate in this small VW layer and propagate to the surface, whereas long-term afterslip arises from the velocity-strengthening (VS) layer beneath it. The continuous creep between successive creep events is due to the existence of the top VS layer. The shallow VS layer might correspond to a special layer observed in sediments in nearby drilling samples (Wei et al., 2013). Detailed studies including well log data in the nearby Salton Sea Geothermal Field found that Salton Trough sediments can switch from failing

Table 1
Triggered slip amplitude on SHF by major regional earthquakes.

Year	M_w	Earthquake	Static perturbations[a] (MPa)	Dynamic perturbations[b] Maximum and minimum dynamic Coulomb stress (MPa)	SHF	
					Maximum slip on SHF (cm)	Distance from earthquake (km)
1968	6.5	Borrego Mountain	0.03[1]	N/A	2.5	40
1979	6.4	Imperial	0.03[1]	0.8 (−0.7)	2.0	45
1981	5.8	Westmorland	0.05[1]	2.9 (−2.4)	1.4	20
1986	6.0	North Palm Springs	< 0.0001[1]	N/A	N/A	139
1992	7.3	Landers	< 0.0001[1,2,3]	0.5 (−0.6)	2.5	155
1994	6.7	Northridge	< 0.0001[1]	N/A	N/A	295
1999	7.1	Hector Mine	< 0.0001[3]	0.5 (−0.5)	2.0	190
2010	7.2	El Mayor-Cucapah	−0.02[5]	1.6 (−1.6)	2.7	85
2012	5.4	Brawley	0.07[4]	0.05 (−0.05)	0.014	15

[a] The main sources: 1: Du et al., 2003; 2: King et al., 1994; 3: Fialko et al., 2002; 4: Hauksson et al., 2013; 5: Toda and Stein, http://supersites.earthobservations.org/Baja_stress.png.

[b] Based on the closest strong motion station. Data were downloaded from http://strongmotioncenter.org/, rotated to normal and shear directions on the SHF, and translated, respectively, to normal and shear stresses by following $\tau = \frac{dD}{dt} / V_g * \mu$, where D is the strong motion data in displacement, V_g is the surface wave's group velocity (3.5 km/s), and μ is the shear modulus (30 GPa).

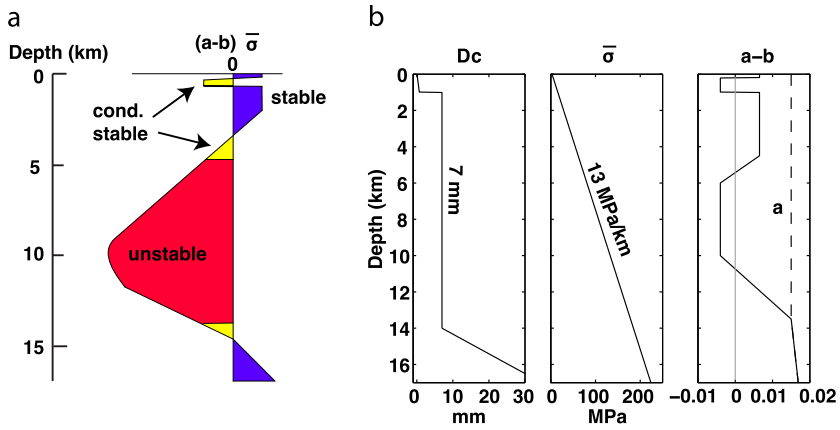

Fig. 4. Physical parameters used in the fault model. (a) Schematic fault model. The yellow, blue, and red regions have conditionally stable, stable, and unstable frictional parameters respectively. (b) Variation of critical distance Dc, effective normal stress $\bar{\sigma}$, friction parameters a–b and a with depth. In the panel titled a–b, the black solid line shows the value of a–b, the dashed line shows the value of a, and the gray line shows a–$b = 0$ to illustrate the changes in frictional stability with depth. (For interpretation of the references to color in this figure legend, the reader is referred to the web version of this article.)

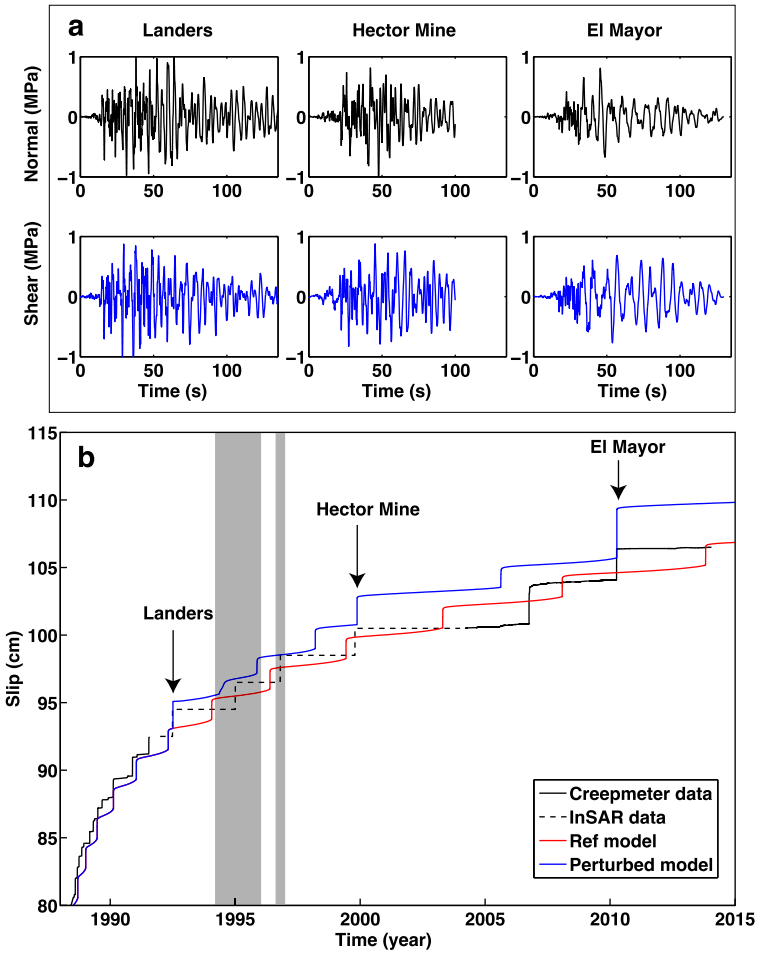

Fig. 5. Numerical simulations and observed surface slip history on the SHF between 1988 and 2015. (a) Dynamic stress perturbations used to produce results in the perturbed model, which are applied at the times of the Landers, Hector Mine, and El Mayor earthquakes. These perturbations are scaled by a factor of 2.13, 2.023, and 0.538 from the stress perturbations derived from the strong motion data at stations 11 628, 11 628, and 11 369, respectively. (b) The red solid line is the reference model with no perturbations added (Wei et al., 2013). The blue line shows a simulation that included all three perturbations. (For interpretation of the references to color in this figure legend, the reader is referred to the web version of this article.)

in creep events to rupturing in earthquakes over just a few km due to hydrothermal alteration and the introduction of a significant amount of feldsphar minerals (McGuire et al., 2015). Similar compositional heterogeneity is possible at the SHF. This fault model can reproduce the geodetic and geological observations, including coseismic slip, rapid afterslip, and spontaneous episodic or continuous creep on the SHF (red line in Fig. 5b; see Wei et al., 2013). Following an earthquake, the rate of displacement contributed by successive creep events decreases continuously, while the interval between events increases before reaching a steady value, consistent with observations. The key parameters in the rate-and-state friction model include a, b, D_c, and $\bar{\sigma}$, where a and b are non-

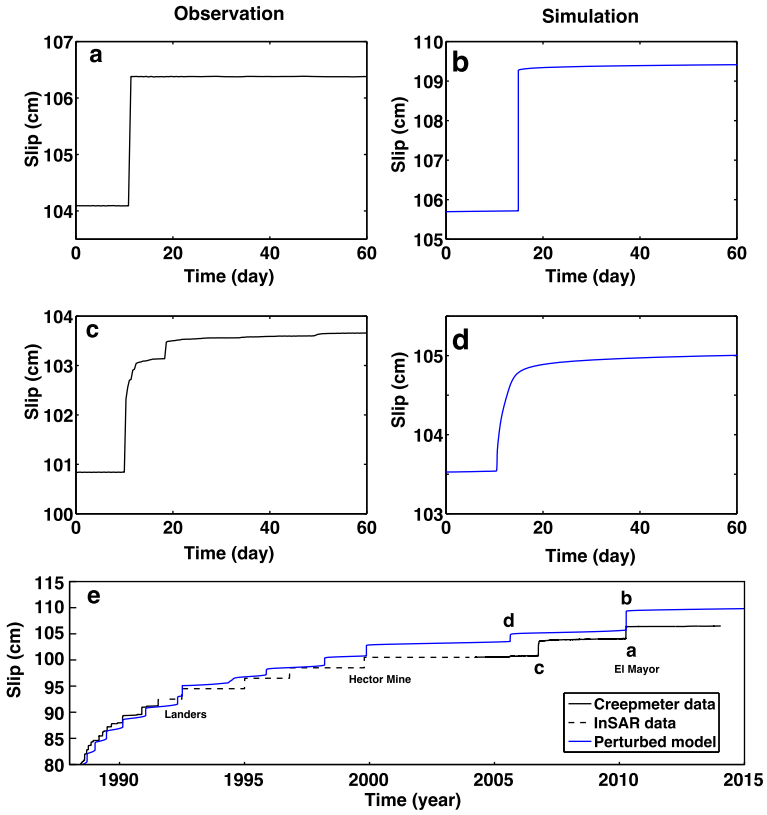

Fig. 6. Creepmeter observations of the triggered event in 2010 (a), and the spontaneous event in 2006 (c), as well as our simulations of the triggered (b), and spontaneous (d) events. (e) Data and simulation, same as Fig. 5b but the reference model (red line in Fig. 5b) is not shown. This figure shows that our model can reproduce the distinct temporal features of both spontaneous and triggered creep events. (For interpretation of the references to color in this figure legend, the reader is referred to the web version of this article.)

dimensional friction stability parameters, D_c is the critical distance (sliding distance required to renew the contact population on the fault following a velocity step), and $\overline{\sigma}$ is the effective normal stress (normal stress minus pore pressure) (Dieterich, 1979; Ruina, 1983). In the shallow VW layer (0.2–1 km depth) (Fig. 4) we set: a–$b = -0.004$; $a = 0.015$; $D_c = 0.2$–0.7 mm; $\overline{\sigma} = 5.6$–15.6 MPa. The effective normal stress increases linearly with depth at a rate of 13 MPa/km (lithostatic minus hydrostatic) and a base value of 2.96 MPa at surface is included.

Normal and shear stress perturbations (static or dynamic) can be applied on the fault at any desired time in the simulated earthquake cycle. For the static cases, we apply the stress change over the entire fault. For the dynamic cases, we apply the perturbations only in the top 3 km where the largest surface wave amplitudes are expected. Fault slip rate and state variable evolution following a stress perturbation are formulated based on laboratory experiments (Linker and Dieterich, 1992; Richardson and Marone, 1999) and are incorporated into the rate-and-state friction model as:

$$\frac{\theta_2}{\theta_1} = \left(\frac{\overline{\sigma}_1}{\overline{\sigma}_2}\right)^{\alpha/b} \tag{1}$$

$$\frac{V_2}{V_1} = \left(\frac{\overline{\sigma}_2}{\overline{\sigma}_1}\right)^{\alpha/a} exp\left(\frac{\tau_2}{a\overline{\sigma}_2} - \frac{\tau_1}{a\overline{\sigma}_1}\right) \tag{2}$$

where θ is the state variable and V is the slip rate. $\overline{\sigma}_1$ and $\overline{\sigma}_2$ are the effective normal stress, and τ_1 and τ_2 are the shear stress, before and after the perturbation, respectively. α is set to be 0.2 for a base friction of 0.6, measured by Linker and Dieterich (1992) and Richardson and Marone (1999) on granite surface with gouge.

Building upon the reference model as shown in Fig. 5b (red solid line), we first added static stress changes up to 0.1 MPa and found that these changes are too small to instantaneously trigger creep events (<0.01 mm slip within 24 h). Then, we applied dynamic perturbations of both normal and shear components, which are constrained by strong motion data from the Landers, Hector Mine, and El Mayor earthquakes (Fig. 5a). As shown in Fig. 5b, the perturbed model (blue solid line) reproduces the observed triggered slip of similar timing and displacement. This indicates that creep events on the SHF are dynamically triggered by these three earthquakes. In addition, there seems to be distinct temporal features between spontaneous and triggered creep events. A spontaneous event includes slip acceleration over a few minutes followed by gradual return to background slip rate over several hours or days, often including multiple small creep events, whereas a triggered event is usually manifested as a single abrupt fault displacement between two data samples (1–5 min). Our model reproduces this feature of the creepmeter data (Fig. 6). The reason for the difference is that when the top VS layer is triggered by the transient dynamic perturbations very little energy is left for afterslip between creep events. Our simulations also show that the same equivalent Coulomb stress change, due to either shear stress only ($\Delta\sigma = 0$) or normal stress only ($\Delta\tau = 0$), would trigger similar creep (Fig. S2 in supplementary materials). This shows that Coulomb stress change is a good indicator for triggering, as was suggested by Perfettini et al. (2003b). In our model, we use a base friction of 0.6 to calculate the Coulomb stress change.

The displacement of triggered creep events scales with the maximum dynamic Coulomb stress change (Fig. 7a). To reproduce the proper displacement for each event, we have to fine-tune the perturbations by applying appropriate scaling factors to the dynamic perturbations derived from strong motion data. Such scaling factors would account for the uncertainties in the calcula-

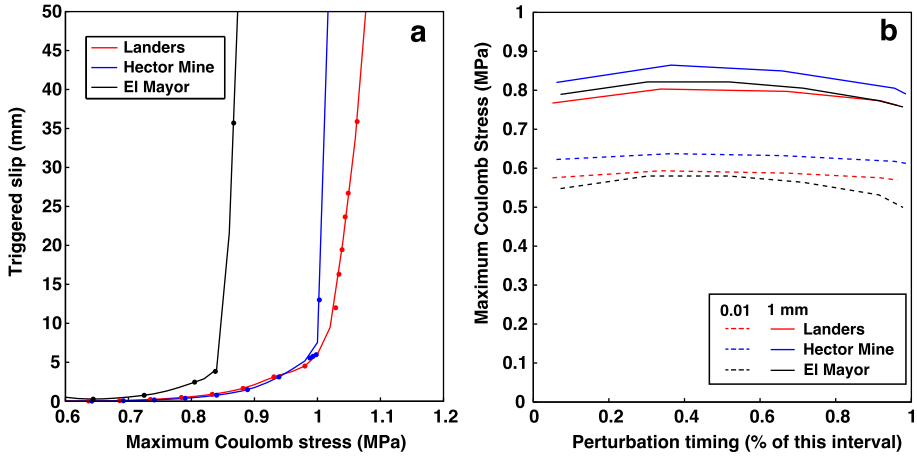

Fig. 7. (a) Relation between the maximum dynamic Coulomb stress change and the amplitude of triggered slip. For each earthquake, we use a perturbation derived from the strong motion station as the reference perturbation. Then we scale the waveform with a range of factors as a group of perturbations to understand the scaling. (b) Coulomb stress threshold for triggering 0.01 mm (dashed lines) and 1 mm (solid lines) of slip events as a function of time during an interval between two successive creep events in our models. For each triggering earthquake, the timing of the perturbation is varied within this interval.

tion of dynamic stress perturbations from strong motion observations, which are not situated directly on the fault, as well as for the uncertainties in the parameters in our rate-and-state model. The modeled displacement scales exponentially with the perturbations until it reaches a threshold, above which the slip scales steeply and linearly with the perturbation and the triggered event becomes an earthquake (maximum velocity >10 cm/s) (Fig. 7a). Thus, if a perturbation is sufficiently strong, the event in the shallow VW layer will become seismic (Kaneko and Lapusta, 2008). The slope of these scaling curves depends on the timing of perturbation. For example, the slope for the Landers case is gentle because the perturbation occurs during an early stage of the creep event cycle. In contrast, the slope for El Mayor is very sharp because the shallow VW layer is close to failure when perturbation is introduced. However, observations show no evidence of triggered earthquakes on SHF from these three mainshock events. Either the perturbation was insufficient to trigger earthquakes or our fault model is missing some physics such as dilatancy strengthening that can stabilize slip (Segall et al., 2010; Liu, 2013) so that the triggered slip will not grow to earthquakes even at very large perturbations.

Based on both observations and numerical simulations we may establish the perturbation threshold needed to trigger creep events on the SHF. Observations (Table S1 in the supplementary materials) show that triggering of creep events on the SHF requires a Mw > 7 earthquake within 150 km, Mw > 6 within 80 km, and Mw > 5 within 20 km. Earthquakes that do trigger creep events on the SHF usually show a peak-to-trough amplitude of 0.5–1 MPa of the dynamic Coulomb stress change, whereas the earthquakes that do not trigger creep events usually have a perturbation less than ~0.01 MPa on the SHF. This brackets the triggering threshold to be somewhere between 0.01–1 MPa. With numerical simulation, we can reduce this triggering threshold uncertainty. Taking the three waveforms in Fig. 5a as examples, we vary the timing of perturbation and scale the waveforms to further constrain the triggering threshold. Because the resolution of the Superstition Hills creepmeter is 9.6 μm during inter-seismic period and 1 mm during co-seismic rupture (Bilham et al., 2004), we plot the stress threshold as a function of time between two spontaneous creep events when the perturbation is introduced for the two resolutions. The triggering threshold for 0.01 mm slip is about 0.6 MPa and the triggering threshold for 1 mm slip is about 0.8 MPa (Fig. 7b). Variation of the threshold with time is small, with the maximum reached around the middle of the interval when the shallow VW layer has returned to a more firmly locked state.

In Fig. 8 we present examples of modeling results for dynamic Coulomb stress histories derived from the Landers earthquake data during the perturbation. We find the triggered creep event usually consists of several individual events, each lasting less than 1 second (blue lines in Fig. 8). The magnitude and timing of each individual event depends on the dynamic Coulomb stress change. Noticeable slip will occur when the Coulomb stress exceeds a threshold, 0.75 MPa for this case, and the displacement depends on the amplitude of the stress above the threshold. Perturbations below this threshold will not trigger any noticeable slip at this scale (red lines in Fig. 8). However, a Coulomb stress change above 0.6 MPa but below 0.75 MPa could trigger small slip at a level of 0.01 mm, which is not visible at the scale presented in Fig. 8c.

The time-integrated dynamic Coulomb stress perturbation also affects the triggering threshold and the displacement of triggered slip, in addition to the maximum Coulomb stress perturbation. In Fig. 9, we show the results of three groups of simulations. Group one is the original waveform for the Landers earthquake. In the other two groups, we modify the original waveform by scaling both the normal and shear stress perturbations by a factor of 0.5 (modified waveform 1, red) and 2 (modified waveform 2, black), respectively, when the Coulomb stress change is negative (Fig. 9a). This multiplication factor artificially reduces or amplifies the negative Coulomb stress change but keeps the positive Coulomb stress change the same for all the three groups. Then we scale each group of perturbation by a common factor of 1.0–2.4 and apply them at timing of the Landers earthquake. The scaling of triggered slip with maximum positive Coulomb perturbation is different for the three groups of simulations (Fig. 9b). Modified waveform 1 requires less Coulomb stress to trigger 1 mm slip whereas modified waveform 2 requires more (Fig. 9d). The threshold scales linearly with the Coulomb stress change integrated over the period of the wave train (Fig. 9d). This shows that the asymmetry of a waveform can also affect the ability to trigger fault creep, in addition to just the maximum Coulomb stress change. The waveform with negative integrated Coulomb stress change (black lines in Fig. 9) can still trigger creep events mainly because the nonlinear effect of stress perturbations on the slip velocity and state variable (as shown in equations (1) and (2)). To our knowledge, there is no previous study on the asymmetry of waveforms for dynamic triggering.

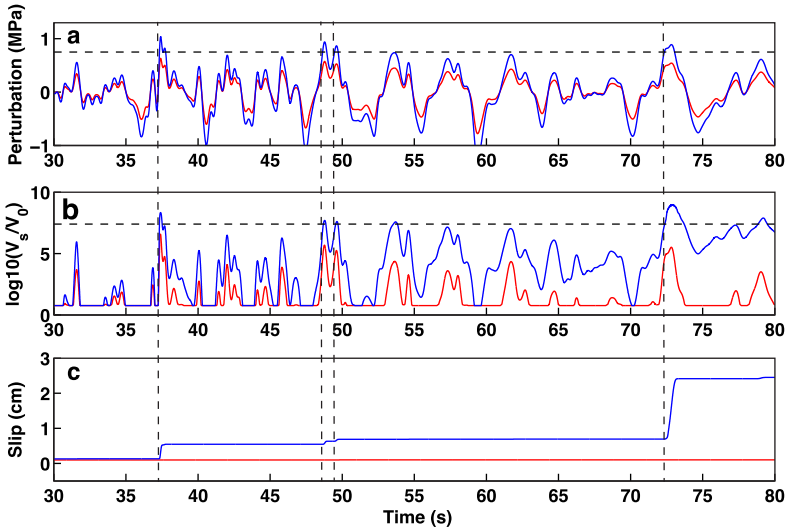

Fig. 8. Effect of Coulomb stress change on the dynamic triggering of modeled creep events during the perturbation. (a) Coulomb stress perturbations applied in cases 1 and 2. Perturbation 1 (blue solid line) is scaled by a factor of 2.13 from the stress perturbation derived from the strong motion data at station 11628 for the Landers earthquake. Perturbation 2 (red solid line) is the same time series scaled up by a factor of 1.30. (b) Modeled surface fault slip velocity V_s (log scale) for the two cases. V_0 is the geological slip rate of SHF at 5 mm/yr. (c) Modeled surface slip resulting from the two perturbations. Horizontal dashed line in (a) shows triggering threshold at 0.75 MPa, and in (b) shows slip velocity V_s at 4 mm/s. Vertical dashed lines are plotted to help identify the phase alignment of noticeable triggered slip. (For interpretation of the references to color in this figure legend, the reader is referred to the web version of this article.)

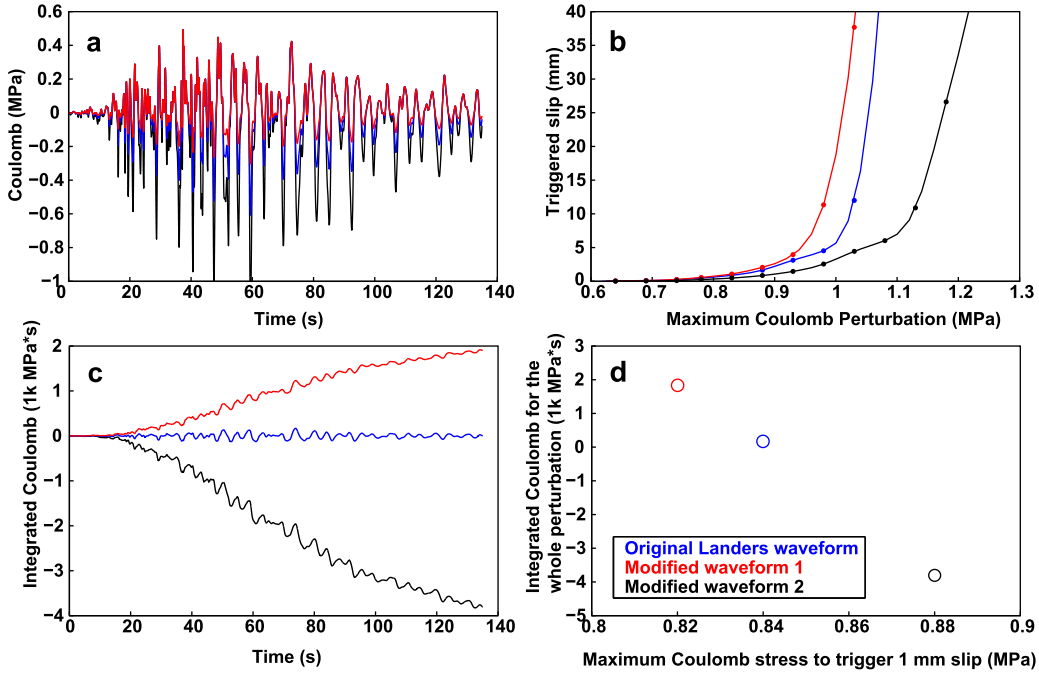

Fig. 9. Effects of perturbations with asymmetric waveforms. (a) Reference perturbations of the three groups of simulations. For each group, we simulated the triggering by perturbations with the same waveform but scaled by different factors ranging from 1.0 to 2.4. (b) Triggered slip versus the maximum Coulomb stress change for the three groups of perturbations (c) Time-integrated Coulomb stress change for the three reference perturbations shown in (a). (d) Coulomb stress change integrated over the period of the wave train of the three reference perturbations scales linearly with the maximum Coulomb stress change needed to trigger 1 mm slip. (For interpretation of the references to color in this figure, the reader is referred to the web version of this article.)

5. Discussion

Perfettini et al. (2003a, 2003b) studied static and dynamic triggering of earthquakes in a 1D fault model in the rate-and-state friction framework. They showed many characteristics that we have seen in our simulations including the instantaneous triggering of slip events. However, in Perfettini et al. (2003b), the instantaneous dynamic triggering threshold is about 7 MPa, whereas ours is an order of magnitude smaller at about 0.6 MPa for 0.01 mm slip and 0.8 MPa for 1 mm slip. This difference likely results from the different parameters used for the fault segments that nucleate the slip events (Table S2 in the supplementary material). The ratio of these thresholds (∼11.7) is close to the ratio of the nucleation sizes in the two studies (∼10; 9 km versus 0.9 km) but not to that of normal stress (∼5) or Dc (∼ 40). However, we find that the triggering threshold does not linearly scale with the nucleation size. We consider three additional scenarios by decreasing (i) the effective normal stress by 50% in the top 1 km, (ii) the Dc by 50% in the top 1 km, and (iii) both the effective normal stress and Dc by 50% (and hence retaining the same $h*$) (Fig. S3 in the sup-

plementary material), where h^* is the nucleation size (Rubin and Ampuero, 2005). The triggering threshold for 1 mm slip decreased from 0.84 to 0.75, 0.78, and 0.74 MPa for scenario (i), (ii), and (iii), respectively (Fig. S3). Therefore, the similar ratio between the triggering threshold and the nucleation size is a coincidence. These results also suggest that the triggering threshold depends on the effective normal stress and Dc even for the same h^*.

The dynamic Coulomb stress model has explained the asymmetry in aftershock distribution of the 1992 Landers earthquake (Kilb et al., 2000), the instantaneously triggering of earthquake in simulations by Perfettini et al. (2003b), and the instantaneously triggering of creep events in our study. This is consistent with what Parsons et al. (2014) have suggested that azimuth and polarization of surface waves might be important for dynamic triggering of earthquakes. The polarization describes the effect when seismic surface waves travel through heterogeneous structure, the wave packets get refracted laterally, away from the source-receiver great circle (Laske et al., 1994), which is different from the polarity of body waves. Both azimuth and polarization of surface waves affect the dynamic Coulomb stress because perturbations caused by surface waves need to be projected to the normal and shear direction of the fault. Therefore, the same surface wave but different azimuth or polarization will cause different dynamic Coulomb stress and triggered slip.

The findings we present in this paper are specific for the SHF site for a specific type of fault slip. It is not yet clear how applicable our results are for other regions. For example, creepmeters in Central California recorded many apparent fault-slip steps at times of moderate local earthquakes of magnitudes 4–5 (King et al., 1977). It is possible to conduct a similar study focusing on Central California. Moreover, the threshold of 0.6 MPa for dynamic triggering for creep events in Salton Trough seems larger than that for triggering earthquakes in geothermal fields, 5 kPa (Brodsky and Prejean, 2005) and non-volcanic tremors in subduction zones, 40 kPa in Cascadia (Rubinstein et al., 2007) and 60 kPa in Taiwan (Peng and Chao, 2008), non-volcanic tremors on San Andreas Fault, 2–3 kPa (Peng et al., 2009), and earthquakes near shale gas production sites in western Alberta, Canada, 0.2–0.4 kPa (Wang et al., 2015). Many remotely triggered earthquakes and non-volcanic tremors are believed to occur at locations with elevated pore pressure and low effective normal stress of a few MPa (Hill et al., 1993; Brodsky and Prejean, 2005; Rubinstein et al., 2007). In contrast, the average normal stress change at the shallow VW layer in our system is much larger at about 10 MPa. Moreover, the different density of source population might also explain the different triggering threshold. As shown in Perfettini et al. (2003b), dynamic triggering threshold drops dramatically if the fault is very close to failure (<5% of interval), i.e. critically stressed. For a given study region, there are much more tremor/earthquake (in geothermal fields) sources that are very close to failure than creep-event sources and hence the observed triggering threshold is much smaller for tremor/earthquake. All in all, if rate-and-state friction is the sole mechanism that dictates triggering, the difference between triggering and non-triggering should depend on the magnitude of the effective normal stress, the frictional properties, or the density of source population of the system.

One key aspect of dynamic triggering as applied to earthquakes and tremor has been the uncertainty in the physical mechanism that would cause the observed delays between the applied stress perturbation and the occurrence of earthquake/tremor event. Shelly et al. (2011) proposed that dynamic triggering of aseismic creep is a likely explanation for the prolonged, dynamically triggered tremor sequences on the deep San Andreas Fault, and by extension for many other delayed triggering earthquake or tremor sequences. Owing to the source depth (~20 km) and small magnitude, those postulated creep events were not detectable with geodetic data and instead inferred based on tremor migration rates (10s of km/h) that are somewhat similar to creep event rupture velocities observed elsewhere. A similar connection is observed in earthquake swarms in the Salton Trough (Lohman and McGuire, 2007; Roland and McGuire, 2009). While the spontaneous creep events on the SHF are not typically associated with any seismicity (Wei et al., 2011), they do propagate at velocities (~100 km/h; Bilham, 1989) similar to that inferred from the tremor migration on the SAF (Shelly et al., 2011). On one hand, this suggests similar frictional properties and stress conditions (Rubin, 2008; Roland and McGuire, 2009) between 20 km depth at Parkfield and top 1 km in Salton Trough. On the other hand, this seems contradictory to our suggestion that effective normal stress can explain the different triggering threshold of tremor at 2–3 kPa (Peng et al., 2009) and creep events at 0.6 MPa (this study).

To look for the connection postulated by Shelly et al. (2011) we examined the seismograms at a nearby seismic station (ERR of the Caltech Regional Seismic Network) during the passing surface waves from the 2004 Mw 9.1 Sumatra, 2010 Mw 8.8 Chile, 2011 Mw 9.0 Tohoku, and 2012 Mw 8.6 Indian Ocean earthquakes which had maximum velocities of 0.06, 0.11, 0.10, and 0.06 cm/s, respectively, but did not trigger any detectable slip on the creepmeter or InSAR data. The corresponding stress perturbations are about 5.1, 9.4, 8.6, and 5.1 kPa. Therefore, the lack of triggered creep is not surprising because the normal stress of the shallow VW layer is quite high (~10 MPa) and these ground motions are at least one order of magnitude smaller than that of the 1992 Landers, 1999 Hector Mine and 2010 El Mayor earthquakes.

Thus, while triggered creep is common on the SHF and other strike-slip faults in the Salton Trough there is not a clear extrapolation of these events as a likely causative source of prolonged tremor or earthquake sequences in other regions. In particular, the observation that triggered creep events happen nearly instantaneously (Fig. 6) in contrast to multi-day spontaneous events suggests that triggered creep may have the same difficulties explaining protracted sequences of triggered seismicity/tremor that last for days following the transient dynamic stresses.

6. Conclusions

Not all creep events on the Superstition Hills fault are triggered by earthquakes, but of the subset that accompany nearby earthquakes we show that dynamic stress changes during the passage of seismic waves are most likely to have triggered slip. Numerical simulations show that static stress changes from regional nearby large earthquakes ($M \geq 5.4$) are typically less than 0.1 MPa and too small to instantaneously trigger creep events, whereas dynamic perturbations alone are large enough to do so. The instantaneous triggering of creep events depends on the peak amplitude of the Coulomb stress change and the time-integrated dynamic Coulomb stress change. Observations show that triggering of creep events on the Superstition Hills fault accompanies $Mw > 7$ earthquakes within 150 km, $Mw > 6$ earthquakes within 80 km, and $Mw > 5$ earthquakes within 20 km. Based on observations and simulations, the stress change amplitude required to trigger a creep event of 0.01 mm surface slip is about 0.6 MPa. This is at least one magnitude larger than the triggering threshold of non-volcanic tremor (2–60 kPa) and earthquakes in geothermal fields (5 kPa) and near shale gas production sites (0.2–0.4 kPa), which may be due to the difference in effective normal stress, friction, or density of source population in these systems or different triggering mechanisms. We conclude that shallow frictional heterogeneity can explain both the spontaneous and dynamically triggered creep events in our study area.

Acknowledgements

We thank Diego Melgar for discussions on high-rate GPS and strong motion instruments. We thank Debi Kilb for a preview of his manuscript. This work was supported by NSF EAR awards 1246966 and 1411704 (M. Wei) and a Canada NSERC Discovery grant (Y. Liu).

Appendix A. Supplementary material

Supplementary material related to this article can be found online at http://dx.doi.org/10.1016/j.epsl.2015.06.044.

References

Allen, C.R., Wyss, M., Brune, J.N., Granz, A., Wallace, R., 1972. Displacements on the Imperial, Superstition Hills, and San Andreas faults triggered by the Borrego Mountain Earthquake, in The Borrego Mountain Earthquake. U. S. Geol. Surv. Prof. Pap. 787, 87–104.

Bilham, R., 1989. Surface slip subsequent to the 24 November 1987 Superstition Hills, California, earthquake monitored by digital creepmeters. Bull. Seismol. Soc. Am. 79, 424–450.

Bilham, R., Suszek, N., Pinkney, S., 2004. California creepmeters. Seismol. Res. Lett. 75, 481–492. http://dx.doi.org/10.1785/gssrl.75.4.481.

Bock, Y., Melgar, D., Crowell, B.W., 2011. Real-time strong-motion broadband displacements from collocated GPS and accelerometers. Bull. Seismol. Soc. Am. 101, 2904–2925. http://dx.doi.org/10.1785/0120110007.

Bodin, P., Bilham, R., Behr, J., Gomberg, J.S., Hudnut, K.W., 1994. Slip triggered on Southern California faults by the 1992 Joshua Tree, Landers, and Big Bear earthquakes. Bull. Seismol. Soc. Am. 84, 806–816.

Boore, D.M., Bommer, J.J., 2005. Processing of strong-motion accelerograms: needs, options and consequences. Soil Dyn. Earthq. Eng. 25, 93–115.

Brodsky, E., Prejean, S.G., 2005. New constraints on mechanisms of remotely triggered seismicity at Long Valley Caldera. J. Geophys. Res. 110, 1–14. http://dx.doi.org/10.1029/2004JB003211.

Cotton, F., Coutant, O., 1997. Dynamic stress variations due to shear faults in plane-layered medium. Geophys. J. Int. 128, 676–688.

Dieterich, J.H., 1979. Modeling of rock friction 1. Experimental results and constitutive equations. J. Geophys. Res. 84, 2161–2168.

Du, W., Sykes, L.R., Shaw, B.E., Scholz, C.H., 2003. Triggered aseismic fault slip from nearby earthquakes, static or dynamic effect? J. Geophys. Res. 108, 1–21. http://dx.doi.org/10.1029/2002JB002008.

Fialko, Y., Sandwell, D., Agnew, D., Simons, M., Shearer, P., Minster, B., 2002. Deformation on nearby faults induced by the 1999 Hector Mine earthquake. Science 297, 1858–1862.

Freed, A.M., 2005. Earthquake triggering by static, dynamic, and postseismic stress transfer. Annu. Rev. Earth Planet. Sci. 33, 335–367. http://dx.doi.org/10.1146/annurev.earth.33.092203.122505.

Gomberg, J., Beeler, N.M., Blanpied, M.L., Bodin, P., 1998. Earthquake triggering by transient and static deformations. J. Geophys. Res. 103, 24411–24426. http://dx.doi.org/10.1029/98JB01125.

Hauksson, E., Stock, J., Bilham, R., Boese, M., Chen, X., Fielding, E.J., Galetzka, J., Hudnut, K.W., Hutton, K., Jones, L.M., Kanamori, H., Shearer, P.M., Steidl, J., Treiman, J., Wei, S., Yang, W., 2013. Report on the August 2012 Brawley earthquake swarm in Imperial Valley, Southern California. Seismol. Res. Lett. 84, 177–189. http://dx.doi.org/10.1785/0220120169.

Hill, D.P., Reasenberg, P.A., Michael, A., Arabaz, W.J., Beroza, G., Brumbaugh, D., Brune, J.N., Castro, R., et al., 1993. Seismicity remotely triggered by the magnitude 7.3 Landers, California, earthquake. Science 260, 1617.

Johnson, P., Savage, H., Knuth, M., Gomberg, J., Marone, C., 2008. The effect of acoustic waves on stick-slip behavior in sheared granular media: implications for earthquake recurrence and triggering. Nature 451, 57–60. http://dx.doi.org/10.1038/nature06440.

Kaneko, Y., Lapusta, N., 2008. Variability of earthquake nucleation in continuum models of rate-and-state faults and implications for aftershock rates. J. Geophys. Res. 113, B12312. http://dx.doi.org/10.1029/2007JB005154.

Kilb, D., Gomberg, J., Bodin, P., 2000. Triggering of earthquake aftershocks by dynamic stresses. Nature 408, 570–574.

King, C.-Y., Nason, R.D., Burford, R.O., 1977. Coseismic steps recorded on creep meters along the San Andreas Fault. J. Geophys. Res. 82, 1655–1662. http://dx.doi.org/10.1029/JB082i011p01655.

King, G.C.P., Stein, R.S., Lin, J., 1994. Static stress changes and the triggering of earthquakes. Bull. Seismol. Soc. Am. 84, 935–953.

Laske, G., Masters, G., Zürn, W., 1994. Frequency-dependent polarization measurements of long-period surface waves and their implications for global phase velocity maps. Phys. Earth Planet. Inter. 84, 111–137.

Lienkaemper, J.J., Galehouse, J.S., Simpson, R.W., 2001. Long-term monitoring of creep rate along the Hayward fault and evidence for a lasting creep response to 1989 Loma Prieta earthquake. Geophys. Res. Lett. 28, 2265–2268.

Linker, M.F., Dieterich, J.H., 1992. Effects of variable normal stress on rock friction: observations and constitutive-equations. J. Geophys. Res. 97, 4923–4940.

Liu, Y., 2013. Numerical simulations on megathrust rupture stabilized under strong dilatancy strengthening in slow slip region. Geophys. Res. Lett. 40, 1311–1316. http://dx.doi.org/10.1002/grl.50298.

Lohman, R.B., McGuire, J.J., 2007. Earthquake swarms driven by aseismic creep in the Salton Trough, California. J. Geophys. Res. 112. http://dx.doi.org/10.1029/2006jb004596.

Louie, J.N., Allen, C.R., Johnson, D.C., Haase, P.C., Cohn, S.N., 1985. Fault slip in southern California. Bull. Seismol. Soc. Am. 75, 811–833.

McGuire, J.J., Lohman, R.B., Catchings, R.D., Rymer, M.J., Goldman, M.R., 2015. Relationships among seismic velocity, metamorphism, and seismic and aseismic fault slip in the Salton Sea Geothermal Field region. J. Geophys. Res. 120, 2600–2615. http://dx.doi.org/10.1002/2014JB011579.

Parsons, T., Segou, M., Marzocchi, W., 2014. Invited review: the global aftershock zone. Tectonophysics 618, 1–34. http://dx.doi.org/10.1016/j.tecto.2014.01.038.

Peng, Z., Chao, K., 2008. Non-volcanic tremor beneath the Central Range in Taiwan triggered by the 2001 Mw 7.8 Kunlun earthquake. Geophys. J. Int. 175, 825–829. http://dx.doi.org/10.1111/j.1365-246X.2008.03886.x.

Peng, Z., Vidale, J.E., Wech, A.G., Nadeau, R.M., Creager, K.C., 2009. Remote triggering of tremor along the San Andreas Fault in central California. J. Geophys. Res. 114, 1–18. http://dx.doi.org/10.1029/2008JB006049.

Perfettini, H., Schmittbuhl, J., Cochard, A., 2003a. Shear and normal load perturbations on a two-dimensional continuous fault: 1. Static triggering. J. Geophys. Res. 108. http://dx.doi.org/10.1029/2002JB001804.

Perfettini, H., Schmittbuhl, J., Cochard, A., 2003b. Shear and normal load perturbations on a two-dimensional continuous fault: 2. Dynamic triggering. J. Geophys. Res. 108. http://dx.doi.org/10.1029/2002JB001805.

Richards-Dinger, K., Stein, R.S., Toda, S., 2010. Decay of aftershock density with distance does not indicate triggering by dynamic stress. Nature 467, 583–586. http://dx.doi.org/10.1038/nature0940.

Richardson, E., Marone, C.J., 1999. Effects of normal stress vibrations on frictional healing. J. Geophys. Res. 104, 28,859–28,878.

Roland, E., McGuire, J.J., 2009. Earthquake swarms on transform faults. Geophys. J. Int. 178, 1677–1690.

Rubin, A.M., 2008. Episodic slow slip events and rate-and-state friction. J. Geophys. Res. 113. http://dx.doi.org/10.1029/2008jb005642.

Rubin, A.M., Ampuero, J.P., 2005. Earthquake nucleation on (aging) rate-and-state faults. J. Geophys. Res. 110, B11312.

Rubinstein, J.L., Vidale, J.E., Gomberg, J., Bodin, P., Creager, K.C., Malone, S.D., 2007. Non-volcanic tremor driven by large transient shear stresses. Nature 448, 579–582. http://dx.doi.org/10.1038/nature06017.

Ruina, A.L., 1983. Slip instability and state variable friction laws. J. Geophys. Res. 88, 10,359–10,370.

Rymer, M.J., Boatwright, J., Seekins, L.C., Douglas Yule, J., Liu, J., 2002. Triggered surface slips in the Salton Trough associated with the 1999 Hector Mine, California, Earthquake. Bull. Seismol. Soc. Am. 92, 1300–1317. http://dx.doi.org/10.1785/0120000935.

Scholz, C., 1998. Earthquakes and friction laws. Nature 391, 37–42. http://dx.doi.org/10.1038/34097.

Schulz, S., Burford, R.O., Mavko, B., 1983. Influence of seismicity and rainfall on episodic creep on the San Andreas fault system in Central California. J. Geophys. Res. 88, 7475–7484.

Segall, P., Rubin, A.M., Bradley, A.M., Rice, J.R., 2010. Dilatant strengthening as a mechanism for slow slip events. J. Geophys. Res. 115, B12305. http://dx.doi.org/10.1029/2010JB007449.

Shelly, D.R., Peng, Z., Hill, D.P., Aiken, C., 2011. Triggered creep as a possible mechanism for delayed dynamic triggering of tremor and earthquakes. Nat. Geosci. 4, 384–388.

Simpson, R.W., Schulz, S.S., Dietz, L.D., Burford, R.O., 1988. The response of creeping parts of the San Andreas fault to earthquakes on nearby faults: two examples. Pure Appl. Geophys. 126, 665–685.

Stein, R.S., 1999. The role of stress transfer in earthquake occurrence. Nature 402, 605–609. http://dx.doi.org/10.1038/45144.

Wang, B., Harrington, R.M., Liu, Y., Yu, H., Carey, A., van der Elst, N.J., 2015. Isolated cases of remote dynamic triggering in Canada detected using cataloged earthquakes combined with a matched-filter approach. Geophys. Res. Lett. 42. http://dx.doi.org/10.1002/2015GL064377.

Wei, M., Sandwell, D., Fialko, Y., Bilham, R., 2011. Slip on faults in the Imperial Valley triggered by the 4 April 2010 Mw 7.2 El Mayor-Cucapah earthquake revealed by InSAR. Geophys. Res. Lett. 38, L01308. http://dx.doi.org/10.1029/2010GL045235.

Wei, M., Kaneko, Y., Liu, Y., McGuire, J.J., 2013. Episodic fault creep events in California controlled by shallow frictional heterogeneity. Nat. Geosci. 6, 1–5. http://dx.doi.org/10.1038/ngeo1835.

Williams, P., Magistrale, H.W., 1989. Slip on the Superstition Hills fault associated with the 24 November 1987 Superstition Hills, California, earthquake. Bull. Seismol. Soc. Am. 79, 390–410.